The Journal of Chemical Physics

Probing the predissociated levels of the S_1 state of acetylene via H-atom fluorescence and photofragment fluorescence action spectroscopy

Cite as: J. Chem. Phys. **149**, 174309 (2018); https://doi.org/10.1063/1.5045046
Submitted: 15 June 2018 . Accepted: 17 October 2018 . Published Online: 05 November 2018

Jun Jiang, Catherine A. Saladrigas, Trevor J. Erickson, Clare L. Keenan, and Robert W. Field

View Online Export Citation CrossMark

ARTICLES YOU MAY BE INTERESTED IN

Slow photoelectron velocity-map imaging of cold C_7^- and C_9^-
The Journal of Chemical Physics **149**, 174306 (2018); https://doi.org/10.1063/1.5054792

Conformer-specific photoionization and conformational stabilities of isobutanal revealed by one-photon mass-analyzed threshold ionization (MATI) spectroscopy
The Journal of Chemical Physics **149**, 174302 (2018); https://doi.org/10.1063/1.5051682

Fundamental vibration frequency and rotational structure of the first excited vibrational level of the molecular helium ion (He_2^+)
The Journal of Chemical Physics **149**, 154302 (2018); https://doi.org/10.1063/1.5051089

Lock-in Amplifiers
Find out more today

Zurich Instruments

AIP Publishing

© 2018 Author(s).

Probing the predissociated levels of the S_1 state of acetylene via H-atom fluorescence and photofragment fluorescence action spectroscopy

Jun Jiang, Catherine A. Saladrigas, Trevor J. Erickson, Clare L. Keenan, and Robert W. Field[a)]
Department of Chemistry, Massachusetts Institute of Technology, Cambridge, Massachusetts 02139, USA

(Received 15 June 2018; accepted 17 October 2018; published online 5 November 2018)

We report two new experimental schemes to obtain rotationally resolved high-resolution spectra of predissociated S_1 acetylene levels in the 47 000-47 300 cm^{-1} energy region (~1200 cm^{-1} above the predissociation threshold). The two new detection schemes are compared to several other detection schemes (employed at similar laser power, molecular beam temperature, and number of signal averages) that have been used in our laboratory to study predissociated S_1 acetylene levels, both in terms of the signal-to-noise ratio (S/N) of the resultant spectra and experimental simplicity. In the first method, H-atoms from the predissociated S_1 acetylene levels are probed by two-photon laser-induced fluorescence (LIF). The H-atoms are pumped to the 3*d* level by the two-photon resonance transition at 205.14 nm. The resulting 3*d*–2*p* fluorescence (654.5 nm) is collected by a photomultiplier. The S/N of the H-atom fluorescence action spectrum is consistently better by ~3× than that of the more widely used H-atom resonance-enhanced multiphoton ionization (REMPI) detection. Laser alignment is also considerably easier in H-atom fluorescence detection than H-atom REMPI detection due to the larger number-density of molecules that can be used in fluorescence *vs*. REMPI detection schemes. In the second method, fluorescence from electronically excited C_2 and C_2H photofragments of S_1 acetylene is detected. In contrast to the H-atom detection schemes, the detected C_2 and C_2H photofragments are produced by the *same* UV laser as is used for the $\tilde{A}$–$\tilde{X}$ acetylene excitation. As a result, laser alignment is greatly simplified for the photofragment fluorescence detection scheme, compared to both H-atom detection schemes. Using the photofragment fluorescence detection method, we are able to obtain action spectra of predissociated S_1 acetylene levels with S/N ~2× better than the HCCH REMPI detection and ~10× better than H-atom and HCCH LIF detection schemes. *Published by AIP Publishing.* https://doi.org/10.1063/1.5045046

I. INTRODUCTION

The study of the first electronically excited singlet (S_1) state of acetylene was reported more than 100 years ago, when Stark and Lipp published the first absorption spectrum of gas-phase acetylene from 2200 to 1900 Å.[1] Classic papers by Ingold and King[2] and by Innes[3] demonstrated that the excited state observed in the absorption spectrum has a *trans*-bent structure (C_{2h} point group) instead of the linear structure ($D_{\infty h}$ point group) of the electronic ground state (S_0). From the observed rotational selection rule, the S_1–S_0 transition was identified as a *c*-type ($\Delta K_a = \pm 1$ and ΔK_c = even) $\tilde{A}^1A_u$–$\tilde{X}^1\Sigma_g$ transition. Detailed analyses[4–16] led to essentially complete vibrational and rotational assignment up to 4500 cm^{-1} above the zero-point level of the S_1 *trans* conformer, and recent work from our group identified several S_1 *cis*-conformer levels.[15,17] The *cis*-conformer levels borrow transition intensity by interaction with nearby S_1 *trans* levels. High-level *ab initio* calculations[18] and effective Hamiltonian fitting of the experimental data[19] have mapped the isomerization path and located the *cis*-*trans* isomerization barrier at ~5000 cm^{-1} above the *trans* minimum energy.

We have encountered both assignment and experimental difficulties in extending the vibrational assignments to levels >4500 cm^{-1} above the S_1 zero-point vibrational level.[20] The *cis*-*trans* isomerization process greatly alters the vibration-rotation energy-level structures of both *trans* and *cis*-conformer levels near the top of the isomerization barrier.[17] Our polyad fit model, based on an effective Hamiltonian for the *trans*-conformer (i.e., the presence of the *cis*-conformer on the potential energy surface is not directly taken into account by the current version of the polyad fit model), fails to accurately predict positions of levels above 4500 cm^{-1}. The appearance of the *cis*-conformer levels in the spectrum further complicates the assignments. In addition, the predissociation threshold of acetylene (46 074 ± 8 cm^{-1})[21] lies ~1000 cm^{-1} below the top of the isomerization barrier. The fluorescence quantum yield of laser-induced fluorescence (LIF) (the most commonly used technique in the study of S_1 acetylene) diminishes greatly for the predissociated levels. As a result, only about half of the expected levels near 5000 cm^{-1} above the *trans*-conformer zero-point level have been observed by LIF. This reduced fluorescence quantum yield, in combination with the partial breakdown of our polyad fit model, makes challenging secure vibrational and conformer assignments of the observed subset of levels.

a)Author to whom correspondence should be addressed: rwfield@mit.edu

TABLE I. Comparison of several high-resolution detection schemes for predissociated S_1 acetylene levels in the 47 000-47 300 cm^{-1} region, in terms of experimental simplicity and quality of the resultant spectra. The simplicity of the detection scheme is largely influenced by whether an additional probe laser beam is required, which is indicated in this table. The quality of the spectrum is quantified based on the S/N of the spectrum taken with various detection schemes, as listed in Tables II and III. The quality of the H-REMPI spectrum, with the lowest S/N, is set to be one in this table.

	PFAS	HFAS	HCCH REMPI	H-REMPI	HCCH LIF
Quality	20	3	10	1	1.5
Additional probe	No	Yes	No	Yes	No

To increase the detection efficiency, resonance-enhanced multi-photon ionization (2 + 1 REMPI) detection of H atoms (H-REMPI) was previously applied in our laboratory.[20] The signal-to-noise ratio (S/N) of H-REMPI detection, however, is not significantly improved relative to acetylene LIF in the energy region of interest (~5000 cm^{-1} above the *trans* minimum and ~1000 cm^{-1} above the predissociation threshold) although H-REMPI does permit observation of one predissociated band that is barely observable by LIF detection. REMPI detection of acetylene (HCCH REMPI) has also been used to study predissociated S_1 levels,[20,22] and the S/N of the resultant spectrum is larger than those of H-atom ion-detection and acetylene LIF.

We report here two new experimental strategies to obtain rotationally resolved high-resolution spectra of predissociated S_1 acetylene levels. In the first method, instead of detecting the H atoms via REMPI, we detect the H-atoms by monitoring two-photon excited laser-induced fluorescence. This method is referred to as H-atom fluorescence action spectroscopy (HFAS). The HFAS detection is an improvement over the more widely used H-REMPI detection, both in terms of the S/N of the resultant H-atom action spectra of S_1 acetylene and experimental convenience, due to larger number-density of molecules that can be used in fluorescence *vs.* REMPI detection schemes. In addition to probing the predissociated S_1 levels, the HFAS method, in combination with HCCH LIF detection, provides rotationally resolved information about the predissociation mechanism in S_1 acetylene. In the second method, fluorescence from the electronically excited C_2 and C_2H photofragments from S_1 acetylene is detected. This second method, referred to as photofragment fluorescence action spectroscopy (PFAS), offers superior S/N, compared to HCCH LIF and the two H-atom detection techniques. It is also the easiest method to implement because a *single* UV laser is used for both S_1–S_0 excitation and the resonance-enhanced (at the one-photon level) multi-photon fragmentation. No additional probe laser beam is needed. A comparison of all the high-resolution detection schemes of predissociated S_1 acetylene that have been used in our laboratory is given in Table I, in which the quality of the resultant spectrum is quantified based on its S/N given in Tables II and III. The simplicity and sensitivity of this scheme may be useful in detecting transitions into predissociated levels of other molecules, which will be discussed in detail in Sec. IV C.

TABLE II. Comparison of S/N of HFAS, H-REMPI, HCCH REMPI, and HCCH LIF spectra for the 3^5 $K = 1$ levels of S_1 acetylene. The size of the noise is taken to be the 2σ value of the baseline noise fluctuation. The S/N of a specific detection scheme into the 3^5 $K = 1$ levels is taken to be the average S/N of the low-J'' transitions: Q(1)-Q(5) and R(0)-R(5).

	HFAS	H-REMPI	HCCH REMPI	HCCH LIF
S/N	160	50	470	70

TABLE III. Comparison of S/N of PFAS and HCCH LIF spectra for IR-UV double-resonance transitions into the $3^2 5^1$ $K = 2$ levels of S_1 acetylene. The size of the noise is taken to be the 2σ value of the baseline noise fluctuation. The S/N of a specific detection scheme into the $3^2 5^1$ $K = 2$ levels is taken to be the average S/N of the R(1)-R(5) transitions.

	PFAS	HCCH LIF
S/N	520	35

II. EXPERIMENTAL DETAILS

Both H-atom and photofragment (C_2 and C_2H) fluorescence detection experiments are carried out in a vacuum chamber fitted with a diffusion pump (Varian, VHS-6), which achieves an ultimate pressure of 10^{-6} torr. A molecular beam of acetylene is expanded through a pulsed valve (General Valve, Series 9, d = 1.0 mm) into the vacuum chamber. A mixture of acetylene (13%) in Ar at 3 atm backing pressure is used in the H-atom experiment, and neat acetylene with 1 atm backing pressure is used in the carbon-fragment detection scheme. Under gas load, the chamber pressure is ~5×10^{-5} torr.

The laser beams used in the experiments are produced by two tunable dye lasers, Lambda Physik FL2002 and FL3002E, pumped, respectively, by the second and third harmonics of a Q-switched, injection-seeded, Nd:YAG laser (Spectra Physics, Pro-270), operating at 20 Hz. Nonlinear processes are applied to generate the desired wavelengths for specific experiments (see Secs. II A and II B). The resulting laser beams intersect the molecular beam ~1.5 cm downstream from the pulsed nozzle orifice (1 mm in diameter). Fluorescence signals, collected by f/1.2 optics, are observed at an angle mutually perpendicular to the laser path and the molecular beam and recorded by a photomultiplier (PMT) (Hamamatsu R375), with appropriate filter choice (see Secs. II A and II B). To minimize scattered laser light in the fluorescence detection, the laser beams enter and exit the chamber through Brewster windows attached at the ends of two one-foot-long arms (30.5 cm), each of which is equipped with two iris baffles (SM1 components, Thorlabs). The PMT signal is split, and one part of it is input to a 30 dB voltage amplifier (Femto DHPVA-200), with 1.8 ns rise-time at 200 MHz bandwidth. The two output signals are monitored simultaneously on a digital oscilloscope (LeCroy, 9360), and the data are transferred to a computer for storage and post-processing.

A. H-atom fluorescence action spectroscopy (HFAS)

Two counter-propagating laser beams are used in the H-atom fluorescence (HFAS) experiments. The pump laser

beam, weakly focused by an f = 50 cm lens, is used to excite an S_1–S_0 acetylene transition to a predissociated S_1 level. To probe the resulting H-atom photofragments, a second focused laser beam (f = 30 cm lens), delayed by 5 ns with respect to the excitation laser pulse, excites the H-atoms into the 3s and 3d levels by a two-photon transition at 205.14 nm. Fluorescence (654.5 nm) from the H-atom 3s and 3d levels into the 2p level is detected by the PMT. A 630 nm long-pass filter (Newport, CGA-630) is used to minimize residual scattered light and fluorescence from photofragments of S_1 acetylene, principally C_2 Swan band emission. The acetylene excitation and H-atom probe scheme is summarized in Fig. 1. Given that the two-photon H-atom 3d ← 1s transition is approximately an order of magnitude stronger than the two-photon 3s ← 1s transition,[23,24] the H-atom fluorescence signals are dominated by the 3d → 2p emission, which has a lifetime of <20 ns.[25] The 3s → 2p emission signal (>100 ns lifetime)[25] is much weaker.

The excitation laser radiation is produced by the FL-3002E dye laser (Stilbene 420 dye). The dye laser output (420-430 nm) is frequency-doubled in a β-barium borate (BBO) crystal, and a small portion of the fundamental is used for $^{130}Te_2$ frequency calibration. An intracavity etalon reduces the spectral width of the dye laser fundamental to 0.04 cm^{-1}, and the UV excitation power is approximately 100 μJ/pulse. The H-atom probe laser beam at 205.14 nm is produced by frequency-tripling the output of the FL2002 dye laser at 615.42 nm (Rhodamine 640 dye). The wavelength of the fundamental beam is monitored by a wavemeter (Wavemaster, Coherent). A combination of two BBO crystals and a zero-order half-wave plate (Thorlabs, WPH05M-308) was used to achieve frequency-tripling. The grating-limited spectral width of the 205 nm beam is 0.15 cm^{-1}, with a pulse-energy of ~500 μJ/pulse.

We emphasize that the power of the UV acetylene S_1–S_0 excitation beam is intentionally kept at a relatively low level (100 μJ/pulse) in the H-atom fluorescence experiment. On each $\tilde{A}$–$\tilde{X}$ resonance, we observe, in addition to the H-atom signal, a long lifetime fluorescence signal, which is not dependent on the presence of the H-atom probe beam. In fact, the intensity of the long lifetime signal can completely overwhelm the H-atom signal if the power of this UV pump laser is >250 μJ/pulse. To minimize the "unwanted" signal (so that it is at least an order of magnitude smaller than the H-atom signal), the UV pump power must be decreased. As discussed in Sec. II B, the "unwanted" signal turns out to be the basis for our second (preferred) strategy for detection of transitions into predissociated S_1 levels.

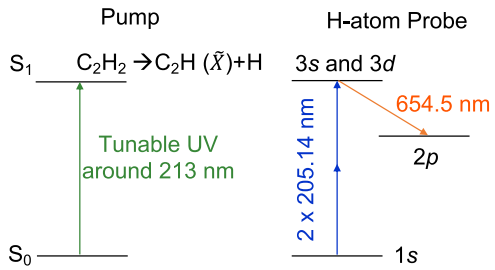

FIG. 1. Level diagrams (not drawn to energy-scale) relevant to the acetylene pump and H-atom probe scheme. H-atom fluorescence signals at 654.5 nm are collected by a PMT.

B. Photofragment fluorescence action spectroscopy (PFAS)

The photofragment fluorescence action spectroscopy technique (PFAS) is based on one-color, multi-photon dissociation of acetylene, resonance-enhanced at the one-photon level by a rotationally resolved $\tilde{A}$–$\tilde{X}$ transition. A single UV laser beam (focused by an f = 70 cm lens) excites the $\tilde{A}$–$\tilde{X}$ transition and also causes photodissociation of S_1 acetylene into electronically excited C_2 and C_2H fragments. Swan band emissions of C_2 and fluorescence of C_2H are detected by the PMT with a 550 nm long-pass filter (Thorlabs, FGL550S). A 2 μs duration fluorescence time-trace is recorded by the oscilloscope and integrated to generate the action spectrum.

Since a single UV laser beam serves both "excitation" and "probe" roles, the laser-alignment process is greatly simplified. This is demonstrated by our successful implementation of an IR-UV double-resonance $\tilde{A}$–$\tilde{X}$ excitation scheme. In that case, the IR laser, focused by an f = 40 cm lens, excites acetylene simultaneously into J = 1–5 f-symmetry rotational levels of the S_0 $\nu_3+\nu_4''$ combination level by Q-branch pumping. A focused UV beam excites the vibrationally excited molecules into a selected S_1 rovibrational level and sequentially produces the photofragment signals. The photofragment detection scheme is summarized in Fig. 2.

The UV excitation beam (230-235 nm) is generated from an etalon-narrowed (0.04 cm^{-1} spectral width) Lambda Physik FL-3002E dye laser (Coumarin 460 dye) and has an energy of approximately 300-400 μJ/pulse. The IR radiation (~2500 nm) is produced by difference frequency generation in a $LiNbO_3$ crystal, using the fundamental of the injection-seeded Nd:YAG laser (1064 nm) and the near IR (740-750 nm) output of the FL-2002 dye laser (LDS 751 dye). The IR radiation has an energy of approximately 1.5 mJ/pulse and a grating-limited spectral width of 0.10 cm^{-1}.

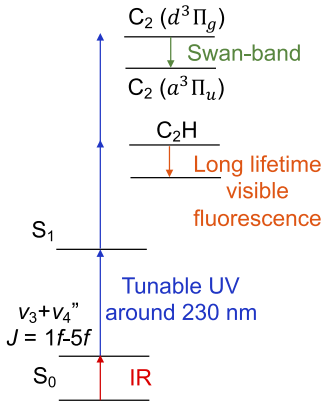

FIG. 2. Level diagram (not drawn to energy-scale) for the photofragment fluorescence detection scheme. The IR laser excites acetylene simultaneously into J = 1–5 f-symmetry rotational levels of the S_0 $\nu_3+\nu_4''$ combination level, by Q-branch pumping. The C_2 $d^3\Pi_g$ state is generated by three same-color UV photons from the IR-populated S_0 $\nu_3+\nu_4''$ levels. The assignment of the electronically excited C_2H fragments is currently unknown although we believe that the fragments are generated by two rather than three UV photons.[26–29] The C_2 Swan-band and C_2H visible emission signals are detected by a PMT.

In applying the PFAS method, it is necessary to consider the possibility of accidental two-photon resonance excitations into high-lying Rydberg states of acetylene. Fortunately, two-photon resonant transitions can usually be distinguished from the target $\tilde{A}$–$\tilde{X}$ transitions because the linewidths of the two-photon resonant transitions are expected to be significantly broader (given the presence of a rapid predissociation channel in the two-photon energy region)[27,28,30–36] than the target one-photon resonant transitions. In the experiment, the UV excitation beam is only weakly focused, i.e., the beam, focused by an f = 70 cm lens, intersects the molecular beam at ~2 cm distance from the UV laser beam waist, to avoid accidental two-photon resonant transitions, none of which have been observed in our acetylene experiments.

III. H-ATOM FLUORESCENCE ACTION SPECTROSCOPY

A. Results

High-resolution HFAS spectra are recorded in the 47 130-47 280 cm^{-1} region (1050-1200 cm^{-1} above the predissociation limit). The S/N of the HFAS spectrum is consistently better by approximately a factor of three than the H-REMPI action spectrum (recorded with similar laser powers), as shown in Fig. 3 for the 3^5 K = 1 levels of S_1 acetylene, where the two action spectra are scaled to a similar noise level. A direct numerical comparison of S/N of HFAS and H-REMPI is given in Table II, which also includes S/N of HCCH REMPI and HCCH LIF detection methods. As mentioned in Sec. I, H-REMPI and HCCH LIF detection schemes yield spectra of similar S/N in the energy region of interest. A higher S/N is now achieved with HFAS detection although it is still not as high as the S/N of HCCH REMPI.

The H-atom fluorescence action spectra, in combination with the LIF spectra (recorded with the same experimental conditions, except that the UV pump beam was unfocused), also allow rotationally resolved study of the predissociation process of S_1 acetylene. We have observed clear evidence of rotational level-dependent predissociation. As indicated by arrows in Fig. 4, the relative intensities of the R(0) and R(1) lines of the $3^4 6^2$ level (magenta) are drastically different in the H-atom and LIF spectra, i.e., in the HFAS spectrum, the R(1) line is ~3× the intensity of the R(0) line, as expected based on the H-atom nuclear-spin statistics, while in the HCCH LIF spectrum, the relative intensities of the two lines are reversed. This indicates that the J = 1 e-symmetry level [reached by the R(0) transition] is more weakly predissociated compared to the J = 2 e-symmetry level [reached by the R(1) transition]. In addition, the predissociation rate seems to be vibrational level-dependent (although the contrast is not as large as the observed rotational dependence in Fig. 4). In Fig. 5, the ratio

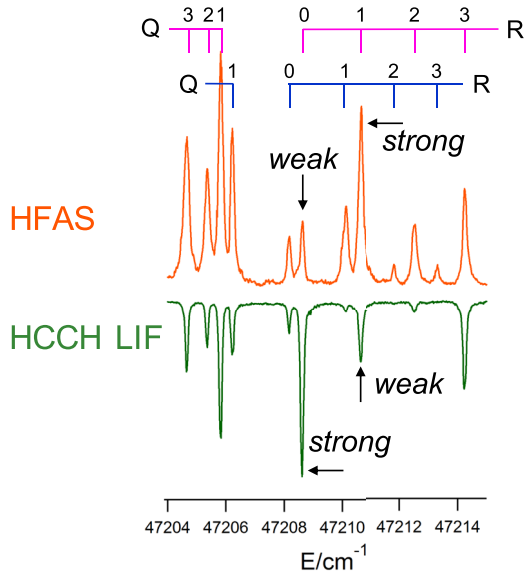

FIG. 4. J-dependent rotational level predissociation. The H-atom fluorescence action spectrum is plotted in orange and the acetylene LIF spectrum in green. Rotational assignments for the two vibrational levels present in this region are given, respectively, by magenta (assigned as the $3^4 6^2$ K = 1 level) and blue tie lines. The vibrational assignment of levels assigned with the blue tie lines is presently undetermined. The arrows are used to emphasize the change in the relative intensities of R(0) and R(1) transitions (indicated by the magenta tie-lines) between the two spectra.

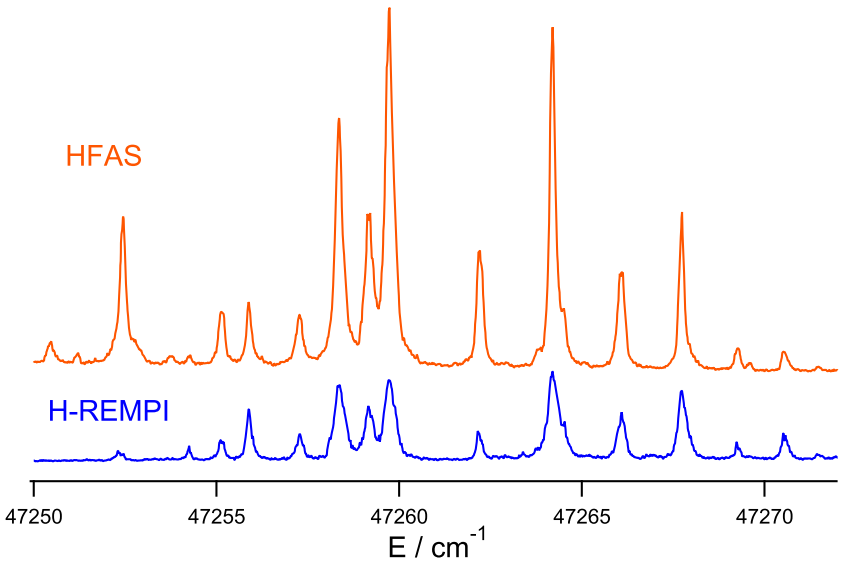

FIG. 3. Comparison of action spectra of 3^5 K = 1 rotational levels of S_1 acetylene, recorded by H-atom fluorescence (orange) and H-atom REMPI (blue) detection schemes. The experimental conditions of the H-atom REMPI detection scheme are described in full detail in Ref. 20. The REMPI spectrum in the figure is recorded with similar excitation and probe laser powers, and the number of signal averages, as the H-atom fluorescence spectrum. The two spectra are scaled to a similar noise level. The figure shows that, on average, the scaled peak intensities are larger by approximately a factor of three in the H-atom fluorescence *vs*. the H-atom REMPI spectra.

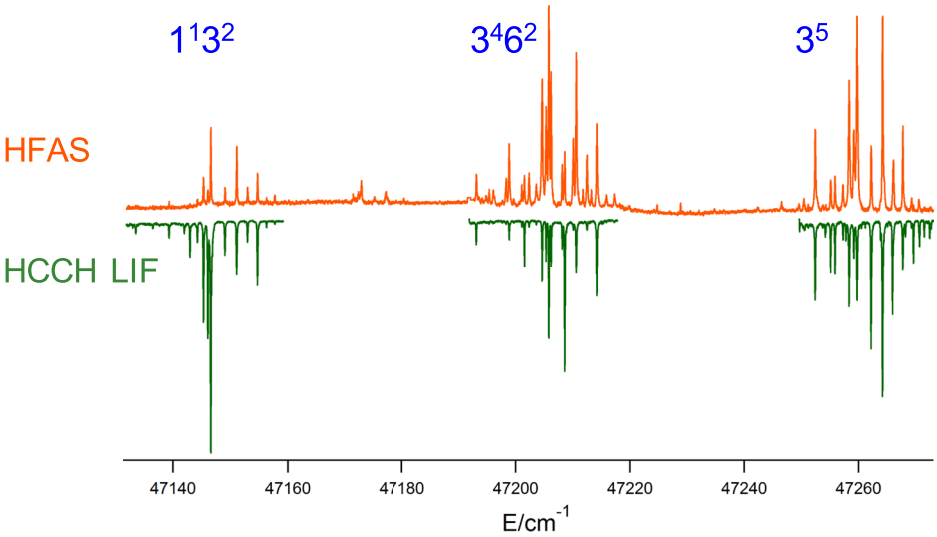

FIG. 5. Vibrational level-dependent predissociation. The H-atom fluorescence action spectrum is plotted in orange and the acetylene LIF spectrum in green. The vibrational level assignments are given above the spectra.

of the HCCH LIF signal to the H-atom signal is larger by a factor of ~2 for the 1^13^2 level (47 147 cm^{-1}) than for the 3^46^2 (47 206 cm^{-1}) and 3^5 (47 260 cm^{-1}) levels. This means that the predissociation rate is slower for 1^13^2 than 3^46^2 and 3^5, even though the three close-lying vibrational levels are all well above the predissociation threshold (46 074 ± 8 cm^{-1}).[21] The observed vibrational and rotational level-dependent predissociation is consistent with a sequential $S_1 \rightarrow T_3 \rightarrow T_2 \rightarrow T_1$ predissociation pathway[37,38] with the T_3-mediated doorway interaction model proposed by Cui and Morokuma.[37] We emphasize that the predissociation process of S_1 acetylene cannot be studied directly using the HCCH REMPI detection, despite the higher S/N of HCCH REMPI spectrum than that of the HFAS spectrum (see Table II).

B. Discussion

The superior S/N of the H-atom fluorescence detection over the H-atom REMPI detection might be surprising, given that REMPI has near-unity detection efficiency, while fluorescence detection efficiency is reduced by both finite detection solid-angle and PMT quantum yield. At the HFAS detection wavelength (654.5 nm), the overall fluorescence detection efficiency in our setup is estimated to be <5% of the overall detection efficiency of REMPI used in Ref. 20. We believe that two factors contribute to the improved S/N in the H-atom fluorescence detection scheme, despite its lower detection efficiency. The total number of acetylene molecules and consequently the total number of H-atoms resulting from the $\tilde{A}$–$\tilde{X}$ excitation are significantly larger in the H-atom fluorescence experiment than the H-atom REMPI experiment because fluorescence detection does not require as low pressure as is needed for REMPI detection (typically operated at $<5 \times 10^{-6}$ torr). We estimate that, based on the pressure of the detection chamber under gas load (5×10^{-5} torr in HFAS *vs.* 5×10^{-6} torr in H-REMPI),[20] the total number of molecules used in our HFAS detection is larger by at least a factor of ten. In addition, the effective linewidth of the probe laser used in the H-atom fluorescence experiment (0.15 cm^{-1}) is about three times larger than that used in the REMPI experiment (0.05 cm^{-1}).[20] Given that the Doppler linewidth of H-atoms from the predissociated S_1 levels of interest is ~3 cm^{-1}[39] and that the focused H-atom probe laser power is high enough to nearly saturate the two-photon transition in both experiments[40] (i.e., $2s \leftarrow 1s$ for H-REMPI and $3d \leftarrow 1s$ for HFAS), the percentage of probed H-atoms is likely higher in the current H-atom fluorescence experiment than in the REMPI experiment by approximately a factor of three.

One of the other advantages of HFAS over H-REMPI detection is that laser alignment is significantly easier in the fluorescence detection scheme than the REMPI scheme. Even though the two detection schemes involve the same number of focused laser beams, with more H-atoms available in the detection chamber, it is considerably easier to achieve good initial laser alignment in the fluorescence detection scheme (the signals can usually be increased by an additional factor of two upon further beam adjustments). In addition, compared to the REMPI scheme, the H-atom fluorescence detection method is applicable in experiments where high-vacuum is not possible, e.g., in a cell (with typical pressure >1 mtorr), or where ion-detection is undesirable, e.g., to avoid stray electric fields >50 mV/cm.

The signal strength could potentially be improved by an order of magnitude if the two-photon Doppler-free detection scheme[41] was applied to probe the H-atoms (e.g., a configuration with two counter-propagating H-atom probe beams), as the Doppler linewidth of the H-atom transition (3 cm^{-1})[39] is significantly wider than the probe laser linewidth (0.15 cm^{-1}).

The limiting factor in the S/N of the current H-atom fluorescence action spectrum is the presence of a non-zero background signal, which is *independent* of the UV pump beam (212 nm) but *dependent* on the presence of both the H-atom probe beam (205 nm) and the acetylene molecules. The background signal has similar fluorescence decay time as the H-atom fluorescence signal that results from acetylene transitions near 212 nm (the $\tilde{A}$–$\tilde{X}$ transitions probed in the experiment), but the background is more sensitive to the power of the 205 nm beam than the desired H-atom signal. It is most likely that the background signal also comes from H-atom fluorescence, and that it is the result of a one-color 1 + 2 process.

The first 205 nm photon excites the acetylene molecule (either resonantly or near-resonantly) into strongly predissociated S_1 levels. The resulting H-atoms are probed by two additional 205 nm photons, which give rise to the constant background signal.

In practice, given that the background signal has a higher-order power dependence on the powerful 205 nm beam than the desired H-atom signal (due to acetylene transitions near 212 nm), the optimal S/N is achieved when the 205 nm probe beam is weakly focused at the center of the molecular beam (i.e., the 205 nm beam interacts with the molecular beam ~1 cm away from the beam waist) so that the background is reduced while the desired H-atom signal still remains strong.

As discussed in Sec. III A, in the energy region of interest, there is an appreciable degree of level-dependence in the S_1 predissociation rate. H-atom, HCCH REMPI, and HCCH LIF detections are sensitive to different types of predissociated S_1 levels. HCCH LIF detection is most suitable for detecting S_1 levels that are weakly predissociated. HCCH REMPI detection, given the high fluence of the focused REMPI laser, is less affected by S_1 predissociation than HCCH LIF detection, but it might not be the best detection scheme for strongly predissociated levels, for which H-atom detection is most suitable. We believe that H-atom, HCCH REMPI, and HCCH LIF detections are complementary detection methods for S_1 acetylene. (The same argument applies to photofragment fluorescence detection, as discussed in Sec. IV.) An improvement in the S/N of the H-atom action spectrum (HFAS *vs*. H-REMPI) is crucial to achieve a complete understanding of the S_1 acetylene level structure and dynamics near the top of the *cis-trans* isomerization barrier, which would involve observations and assignments of much weaker transitions (by at least an order of magnitude) than those into the 3^5 $K = 1$ levels shown in Fig. 3, e.g., nominally forbidden transitions into the S_1 *cis*-conformer levels.

IV. PHOTOFRAGMENT FLUORESCENCE ACTION SPECTROSCOPY

A. Results

Given that a *single* UV laser beam is used for both $\tilde{A}$–$\tilde{X}$ excitation and photo-fragmentation, the photofragment fluorescence detection method is exceptionally easy to implement. Even IR-UV double-resonance $\tilde{A}$–$\tilde{X}$ excitation, which is challenging to apply in the H-atom fluorescence detection (because it requires precise alignment of a focused UV probe laser and two focused IR and UV pump beams), can be easily implemented in the PFAS scheme. The IR-UV double-resonance spectra provide assignment-essential information about the ungerade S_1 vibrational levels, which are inaccessible by single-resonance UV excitation.

The PFAS scheme yields high-resolution IR-UV double-resonance action spectra of ungerade vibrational levels of S_1 acetylene in the 46 700-47 300 cm^{-1} region, which lies 600-1200 cm^{-1} above the predissociation limit. As shown in Fig. 6(a), transitions into $1^1 2^1 B^1$ (where the notation, B^1, indicates that this level belongs to a strongly Coriolis-coupled $1^1 2^1 4^1$–$1^1 2^1 6^1$ bending polyad) $K = 0$ rotational levels (47 186 cm^{-1}) are much more prominent in the PFAS spectrum

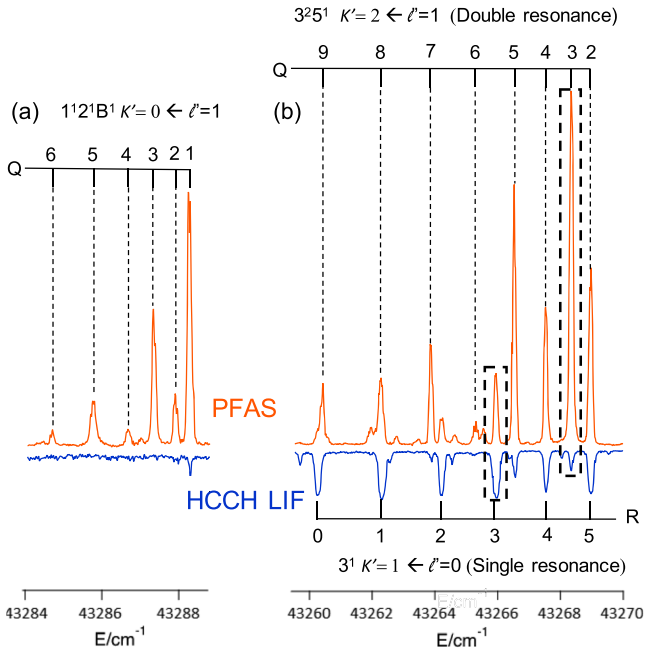

FIG. 6. Spectra recorded with PFAS (upward, orange) and HCCH LIF (downward, blue) detections. Horizontal axes denote the energy of the UV-photon used in the IR-UV double-resonance excitation scheme. Rotational assignments are indicated by vertical lines. (a) IR-UV double-resonance excitation spectrum of the $1^1 2^1 B^1$ $K = 0$ level. (b) IR-UV double-resonance excitation spectrum of the $3^2 5^1$ $K = 2$ level (only the Q-branch spectrum is shown). The IR-UV double-resonance spectrum accidentally overlaps with the *R*-branch of strong single-resonance excitations into 3^1 $K = 1$ rotational levels. In the HCCH LIF spectrum in panel (b), signals from the single-resonance transitions have saturated the oscilloscope. In addition, only the early (20 ns) fluorescence time-window is integrated to generate the HCCH LIF spectrum. This early time-window is of significantly shorter duration than the lifetime of the non-predissociated 3^1 level (~200 ns) but includes essentially the entire duration of the LIF signal from the predissociated $3^2 5^1$ level.

compared to the LIF spectrum, i.e., only the Q(1) transition is observed in the LIF spectrum. A numerical comparison with HCCH LIF detection is given in Table III, which includes S/N of transitions into the $3^2 5^1$ $K = 2$ levels of S_1 acetylene. The S/N of PFAS detection is ~15× larger than that of HCCH LIF. This piece of information, in combination with information provided in Table II, allows us to estimate the quality of all five detection schemes of S_1 acetylene levels, summarized already in Table I. Compared to HCCH LIF, HFAS, and H-REMPI, the PFAS method has significantly higher S/N. The quality of PFAS spectrum is also superior to that of HCCH REMPI by approximately a factor of two.

The PFAS signals are observed for levels both below and above the predissociation limit. In the UV scan region of Fig. 6(b), there exists both IR-UV double-resonance transitions into $3^2 5^1$ $K = 2$ rotational levels (~1000 cm^{-1} *above* the predissociation threshold) and *accidental* single-resonance (UV) transitions into 3^1 $K = 1$ rotational levels (~2000 cm^{-1} *below* the predissociation threshold). Level diagrams associated with the two types of transitions are shown in Fig. 7. Without predissociation, the UV transitions in the IR-UV double-resonance excitation are expected to be approximately an order of magnitude stronger than the single-resonance UV transition, based on the observed Franck-Condon progression in ν_3'.[2,42,43] As we can see from Fig. 6(b) (specifically,

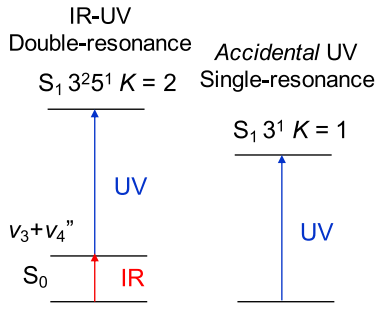

FIG. 7. Level diagrams of IR-UV double resonance transitions into S_1 $3^2 5^1$ $K = 2$ levels and *accidental* single-resonance UV transitions into S_1 3^1 $K = 1$ levels.

the two transitions enclosed in dashed boxes), in the PFAS spectrum, the intensity of the $3^2 5^1$ Q(3) peak with IR-UV double-resonance excitation is ~5× stronger than the intensity of the 3^1 R(3) peak with UV single-resonance excitation, in agreement with expectation based on the ν_3' Franck-Condon progression. In the HCCH LIF spectrum, the relative intensity of the two peaks is reversed. In fact, the intensity of the R(3) transition into the non-predissociated 3^1 vibrational level would have been more than an order of magnitude stronger than the intensity of the Q(3) transition into the predissociated $3^2 5^1$ level, if the signal from the former transition had not saturated the oscilloscope and a longer fluorescence time-window had been used to generate the spectrum. Our analysis of the PFAS and HCCH LIF spectra in Fig. 6(b) thus suggests that while the HCCH LIF signals are strongly affected by predissociation, the PFAS signals are not. At the laser fluence used in our experiment (7 ns, 130 mJ/mm^2), the rate of S_1 photodissociation appears to be faster than the rate of predissociation, which has a typical lifetime of ~10 ns in the energy region of interest, estimated based on the rise time of the H-atom REMPI signal measured in a pump-probe time delay experiment.[39] As discussed in Sec. III B, for S_1 acetylene levels with predissociation rate faster than the photodissociation rate (at the laser fluence currently used in the experiment), PFAS detection efficiency would decrease. However, given that H-atom detection is more challenging to implement, especially in an IR-UV double-resonance excitation scheme, PFAS is currently our best and preferred detection scheme for predissociated S_1 acetylene levels.

B. Discussion

Due to the large difference in wavelengths between the excitation laser (212-235 nm) and the detected fluorescence (visible), scattered laser light can be essentially eliminated in the PFAS detection scheme. This significantly reduces the noise level in the PFAS detection. In comparison, both LIF and H-atom fluorescence detection of predissociated S_1 levels suffer from a significant background signal. Due to the similarity in wavelength between the UV excitation and fluorescence wavelength (<100 nm apart) as well as the short lifetime of the LIF signal (which precludes time-gating of the fluorescence), it is difficult to minimize the background UV scattered light in the LIF detection scheme. The background in the H-atom fluorescence scheme has been discussed in Sec. II A, and it is intrinsic to the technique and the molecular system studied although it can be minimized by using a lower H-atom probe power density.

The spectroscopic characters of the PFAS signals are briefly discussed below. Detailed investigations of the mechanisms of the PFAS signals will be reported in a future publication.[29] The PFAS signals are in the visible region. In comparison, fluorescence from the S_1 levels is concentrated around 300 nm although this fluorescence does extend weakly into the visible. It has a non-linear dependence on the power of the $\tilde{A}$–$\tilde{X}$ pump laser (power-index of 1.6, which implies some laser-saturation effect). The time-dependence of the PFAS signal has at least a bi-exponential decay pattern, with ~120 ns and ~2 μs decay times, respectively. In comparison, LIF signals from predissociated S_1 levels have sub-10 ns lifetimes. There appears to be an additional fast decay process present in the PFAS signal (~30 ns), but it is difficult to determine the lifetime accurately from the recorded 2 μs-long signal.

By dispersing the visible fluorescence using a monochromator, as well as careful analysis of the undispersed PFAS fluorescence time-traces (both of which will be discussed in a follow-up paper),[29] we show that one-color multi-photon excitation of acetylene results in three main emission features. The strongest feature is due to C_2 Swan-band emission ($d^3\Pi_g$–$a^3\Pi_u$, which corresponds to the observed 120 ns decay), centered at 470 nm followed by weaker C_2 Deslandres-d'Azambuja band emission centered around 380 nm ($C^1\Pi_g$–$A^1\Pi_u$, which corresponds to the fastest decay). Underlying the strong discrete features is a near-continuum long lifetime (>2 μs) background emission, the intensity of which grows steadily from 400 nm to the red. The long lifetime visible fluorescence has been observed in previous vacuum-ultraviolet photodissociation studies of acetylene[26–28] and was attributed to C_2H emission. To our knowledge, none of the available *ab initio* calculations, e.g., Refs. 28 and 44, have yielded unambiguous assignments of the observed electronic transitions. It seems likely that the filter choice in our initial PFAS experiments is far from optimal. Nevertheless, the S/N of the PFAS spectra with a 550 nm long-pass filter is already superior to the S/N in all other techniques that we have applied to the S_1 predissociated levels.

The most likely path for the generation of the detected photofragments is as follows: the acetylene molecules are pumped by the initial UV excitation into an S_1 level. The same focused UV beam (which competes with S_1 predissociation) immediately excites the S_1 molecule into the ~90 000 cm^{-1} energy region, where a fast dissociation channel into electronically excited C_2H is known to exist.[27,28,30–36] The resulting C_2H fragments (which are long-lived) are subsequently excited by another UV photon into even higher-lying states, which dissociate into the $d^3\Pi_g$ and $C^1\Pi_g$ states of C_2.

Given the observed intensity of the photofragment emission signals, photodissociation by excitation from the acetylene S_1 state must be efficient. The C_2 Swan band fluorescence detection scheme for acetylene, in particular, is expected to be sensitive even at ~1 atm. Unfortunately, as pointed out by Professor Barney Ellison of the University of Colorado Boulder, the C_2 fluorescence detection might not be a generally applicable detection method for substituted acetylene

due to the possibility of several competing photofragmentation pathways, which are lower in energy than the production of C_2.[45] For example, photofragmentation of CH_3CH_2–CCH to produce C_2 is likely hindered by the possibility of producing HCC–CH_2 and HCC–CH–CH_3 radicals, both of which are stabilized due to electron delocalization among the three carbon atoms in the ·C–CC configuration.

C. General PFAS detection schemes for other molecular systems

While our C_2 and C_2H fluorescence detection schemes might be unique to acetylene, we believe that the one-color PFAS scheme could potentially be a sensitive detection method for predissociated levels of other molecular species. A few possibilities of molecular systems are given in Table IV. Among the eight molecules included in the table, the $\tilde{A} \leftarrow \tilde{X}$ transitions of C_2H_2 (this work) and HNCO[46] have been observed with the PFAS technique. All of the PFAS schemes listed in Table IV are 1 + 1 photodissociation processes, in which the second photon produces fluorescing photofragments from the electronically excited state of the parent molecule prepared by the first photon.

The PFAS detection scheme discussed in this work is different from the Photofragment Fluorescence Excitation (PHOFEX) detection in which photofragments are probed by LIF detection using an additional probe laser, for example, the HFAS detection scheme for acetylene is discussed in Sec. III. Compared to the one-color PFAS scheme, PHOFEX detection has been widely used to detect predissociated molecular levels, e.g., HCO $\tilde{A}$ state (CO A–X),[47] H_2CO $\tilde{A}$ state (HCO B–X),[48] HNCO $\tilde{A}$ state (NH A–X),[46,49] C_2N_2 $\tilde{A}$ state (CN B–X),[50] HCP $\tilde{A}$ and $\tilde{B}$ states (CP B–X),[51] etc., where the appropriate LIF probe transitions of the photofragments are given in parentheses. We believe that while PHOFEX detection is a more generally applicable detection scheme for predissociated levels than PFAS, PFAS detection has the advantage of simplicity since it requires only one laser. In addition, given that only a small number (typically only one) of LIF transitions of the photofragments are probed simultaneously in the PHOFEX scheme, the sensitivity of PHOFEX would be significantly reduced if the photofragments were generated at high rotational and vibrational excitation. By comparison, in the PFAS scheme, visible and UV fluorescence signals from *all* of the rotation-vibration levels of the photofragments are simultaneously detected. The PFAS scheme, however, involves at least one additional transition to a predissociated state. Such a free ← bound transition is generally weaker than a bound ← bound LIF probe transition used in PHOFEX.

Whereas PHOFEX detection applies only to predissociated molecular levels, PFAS detection could be used as a sensitive probe for both predissociated and non-predissociated levels, as demonstrated in Fig. 6(b) for PFAS detection of the acetylene S_1 state. Similar to REMPI detection, the PFAS detection efficiency is expected to be low for strongly predissociated levels. It is important to note that PFAS detection, which is referred to as multiphoton fluorescence spectroscopy in Ref. 46, has been successfully implemented to detect HNCO $\tilde{A}$-state levels with lifetimes as short as 0.5–1 ps[52] at 3 mJ/pulse of a focused laser beam.

Given that the photodissociation products of molecules with more than four atoms are generally more difficult to predict than those of triatomic and tetratomic molecules, due to the presence of multiple competing dissociation channels, as in the case of the substituted acetylene molecules discussed in Sec. IV B, we choose not to provide a detailed discussion of the use of PFAS for larger molecules here. However, given the experimental simplicity of the PFAS detection scheme, its use merits further experimental investigation, especially when the electronically excited state of the target molecule has partially resolved rotational structure (~1 ps lifetime), e.g., the $\tilde{A}$ state of NC–C_2H (cyanoacetylene), C_2H–CHO (propynal), HCO–HCO (glyoxal), C_2H_3–CHO (acrolein), 1,4-$C_4H_4N_2$ (pyrazine), 1,3-$C_4H_4N_2$ (pyrimidine), 1,2-$C_4H_4N_2$ (pyridazine), and C_6H_6 (benzene) (according to Appendix VI of Ref. 53). The utility of PFAS detection for these larger molecules could be verified by exploring a few filter choices for the PMT detection.

TABLE IV. A few examples of molecular transitions potentially suitable for PFAS detection. With the exception of the CS_2 $\tilde{A}$ state and the HNCO $\tilde{A}$ state, the onset of predissociation occurs at energy above the electronic origin of the upper state of the electronic transitions included in the table. For CS_2 and HNCO, the λ values correspond to the transition wavelength of the respective electronic origin bands. For the other six molecules, λ corresponds to the laser wavelength at the onset of predissociation. λ_{em} gives the approximate range of emission wavelength of the photofragment.

Molecule	Transition	λ/nm	Detection	λ_{em}/nm
HCP	$\tilde{A}/\tilde{B} \leftarrow \tilde{X}$	240	CP $B \rightarrow X$	~350
CS_2	$\tilde{A} \leftarrow \tilde{X}$	216	CS $A \rightarrow X$	~260
SO_2	$\tilde{C} \leftarrow \tilde{X}$	219	SO $A/B \rightarrow X$	~240/260
NCO	$\tilde{A}/\tilde{B} \leftarrow \tilde{X}$	317	CN $B \rightarrow X$	~390
C_2H_2	$\tilde{A} \leftarrow \tilde{X}$	217	C_2H	>400
H_2CO	$\tilde{A} \leftarrow \tilde{X}$	330	HCO $A \rightarrow X$	>600
HNCO	$\tilde{A} \leftarrow \tilde{X}$	308	NCO $A \rightarrow X$	~440
C_2N_2	$\tilde{A} \leftarrow \tilde{X}$	212	CN $B \rightarrow X$	~390

V. CONCLUSION

We introduce two new experimental detection schemes to obtain rotationally resolved action spectra of predissociated S_1 acetylene rotation-vibration levels. The development of these two experimental techniques is essential to an extension of the ongoing study of the S_1 *cis-trans* isomerization process, which has been hindered by the reduction in LIF fluorescence intensity due to S_1 predissociation.

H-atom fluorescence detection is superior to the more widely used H-atom REMPI detection, both in terms of improved S/N and experimental convenience. It is also valuable for characterizing the predissociation mechanisms of the S_1 state of acetylene. The H-atom fluorescence detection scheme can be easily applied to other predissociated molecular systems, in which H-atoms are produced.

The photofragment (C_2 and C_2H) fluorescence detection scheme provides the highest S/N among all of the techniques used in our experiments (LIF, H-atom fluorescence, H-atom REMPI, and HCCH REMPI detection) to study predissociated S_1 levels in the 47 000 cm^{-1} region. The PFAS technique

is easy to implement *because only a single UV laser beam is used for both $\tilde{A}$–$\tilde{X}$ excitation and photodissociation* to produce electronically excited C_2 and C_2H. The superior S/N of the PFAS method relies on the high efficiency of multiphoton dissociation from S_1 acetylene to produce fluorescing photofragments, the mechanism of which will be discussed in a future publication.[29] In addition, we believe that the PFAS detection scheme can be a sensitive detection method for a variety of other molecular systems.

ACKNOWLEDGMENTS

The authors thank Professor Barney Ellison, Professor Joshua Baraban, Tim Barnum, and Professor Anthony Merer for valuable discussions. This material is based on the work supported by the U.S. Department of Energy, Office of Science, Chemical Sciences, Geosciences, and Biosciences Division of the Basic Energy Sciences Office, under Award No. DE-FG0287ER13671.

[1] J. Stark and P. Lipp, Z. Phys. Chem. **86**, 36 (1913).
[2] C. Ingold and G. King, J. Chem. Soc. **1953**, 2702.
[3] K. K. Innes, J. Chem. Phys. **22**, 863 (1954).
[4] J. Watson, M. Herman, J. Van Craen, and R. Colin, J. Mol. Spectrosc. **95**, 101 (1982).
[5] J. Van Craen, M. Herman, R. Colin, and J. Watson, J. Mol. Spectrosc. **111**, 185 (1985).
[6] J. Van Craen, M. Herman, R. Colin, and J. Watson, J. Mol. Spectrosc. **119**, 137 (1986).
[7] A. Utz, J. Tobiason, E. Carrasquillo M., L. Sanders, and F. Crim, J. Chem. Phys. **98**, 2742 (1993).
[8] J. Tobiason, A. Utz, and F. Crim, J. Chem. Phys. **99**, 928 (1993).
[9] M. Mizoguchi, N. Yamakita, S. Tsuchiya, A. Iwasaki, K. Hoshina, and K. Yamanouchi, J. Phys. Chem. A **104**, 10212 (2000).
[10] A. J. Merer, N. Yamakita, S. Tsuchiya, J. F. Stanton, Z. Duan, and R. W. Field, Mol. Phys. **101**, 663 (2003).
[11] A. H. Steeves, A. J. Merer, H. A. Bechtel, A. R. Beck, and R. W. Field, Mol. Phys. **106**, 1867 (2008).
[12] A. J. Merer, N. Yamakita, S. Tsuchiya, A. H. Steeves, H. A. Bechtel, and R. W. Field, J. Chem. Phys. **129**, 054304 (2008).
[13] A. J. Merer, Z. Duan, R. W. Field, and J. K. Watson, Can. J. Phys. **87**, 437 (2009).
[14] A. H. Steeves, H. A. Bechtel, A. J. Merer, N. Yamakita, S. Tsuchiya, and R. W. Field, J. Mol. Spectrosc. **256**, 256 (2009).
[15] J. H. Baraban, P. B. Changala, A. J. Merer, A. H. Steeves, H. A. Bechtel, and R. W. Field, Mol. Phys. **110**, 2707 (2012).
[16] J. Jiang, J. H. Baraban, G. B. Park, M. L. Clark, and R. W. Field, J. Phys. Chem. A **117**, 13696 (2013).
[17] A. J. Merer, A. H. Steeves, J. H. Baraban, H. A. Bechtel, and R. W. Field, J. Chem. Phys. **134**, 244310 (2011).
[18] J. H. Baraban, D. A. Matthews, and J. F. Stanton, J. Chem. Phys. **144**, 111102 (2016).
[19] J. H. Baraban, P. B. Changala, G. C. Mellau, J. F. Stanton, A. J. Merer, and R. W. Field, Science **350**, 1338 (2015).
[20] P. B. Changala, J. H. Baraban, A. J. Merer, and R. W. Field, J. Chem. Phys. **143**, 084310 (2015).
[21] D. H. Mordaunt and M. N. Ashfold, J. Chem. Phys. **101**, 2630 (1994).
[22] K. Tsuji, C. Terauchi, K. Shibuya, and S. Tsuchiya, Chem. Phys. Lett. **306**, 41 (1999).
[23] Y. Gontier and M. Trahin, Phys. Lett. A **36**, 463 (1971).
[24] P. Verkerk, M. Pinard, F. Biraben, and G. Grynberg, Opt. Commun. **72**, 202 (1989).
[25] W. Wiese and J. Fuhr, J. Phys. Chem. Ref. Data **38**, 565 (2009).
[26] M. Suto and L. Lee, J. Chem. Phys. **80**, 4824 (1984).
[27] A. Campos, S. Boye, P. Brechignac, S. Douin, C. Fellows, N. Shafizadeh, and D. Gauyacq, Chem. Phys. Lett. **314**, 91 (1999).
[28] S. Boyé, A. Campos, S. Douin, C. Fellows, D. Gauyacq, N. Shafizadeh, P. Halvick, and M. Boggio-Pasqua, J. Chem. Phys. **116**, 8843 (2002).
[29] J. Jiang, A. Muthike, and R. W. Field, "One-color (212-220 nm), resonance-enhanced (S_1–S_0), multi-photon dissociation of acetylene" (unpublished).
[30] J. K. Lundberg, Y. Chen, J.-P. Pique, and R. W. Field, J. Mol. Spectrosc. **156**, 104 (1992).
[31] J. Lievin, J. Mol. Spectrosc. **156**, 123 (1992).
[32] F. Laruelle, S. Boyé-Péronne, D. Gauyacq, and J. Liévin, J. Phys. Chem. A **113**, 13210 (2009).
[33] M. Ashfold, B. Tutcher, B. Yang, Z. Jin, and S. Anderson, J. Chem. Phys. **87**, 5105 (1987).
[34] K. Tsuji, N. Arakawa, A. Kawai, and K. Shibuya, J. Phys. Chem. A **106**, 747 (2002).
[35] K. Tsuji, K. Misawa, J. Awamura, A. Kawai, and K. Shibuya, J. Phys. Chem. A **117**, 1420 (2013).
[36] J. K. Lundberg, D. M. Jonas, B. Rajaram, Y. Chen, and R. W. Field, J. Chem. Phys. **97**, 7180 (1992).
[37] Q. Cui and K. Morokuma, Chem. Phys. Lett. **272**, 319 (1997).
[38] D. H. Mordaunt, M. N. Ashfold, R. N. Dixon, P. Löffler, L. Schnieder, and K. H. Welge, J. Chem. Phys. **108**, 519 (1998).
[39] T. Suzuki and N. Hashimoto, J. Chem. Phys. **110**, 2042 (1999).
[40] Based on the calculated two-photon transition matrix elements of $2s \leftarrow 1s$ and $3d \leftarrow 1s$ transitions from Ref. 23 and the pulse energy, width, and focusing conditions used in the H-REMPI and HFAS experiments, the peak two-photon Rabi frequency of both transitions will be ~300 MHz, if both H-atom probe lasers operated at a single longitudinal mode and had a Gaussian beam profile. The Sirah laser used in H-REMPI typically operates with one or two dominant longitudinal modes at any laser shot. This means that in the H-REMPI experiment, the peak two-photon Rabi frequency of the H-atom $2s \leftarrow 1s$ transition is ~200 MHz. The Lambda-Physik FL2002 laser used in HFAS operates with approximately five longtitudinal modes at each laser shot. This means that in the HFAS experiment, the peak two-photon Rabi frequency of the H-atom $3d \leftarrow 1s$ transition is ~70 MHz. According to our simulation of the optical Bloch equation which takes into account the spatial profile of the laser beam, with these two estimated peak two-photon Rabi frequencies, on *two–photon* resonance, ~25% of the H-atoms are excited in the $3d \leftarrow 1s$ probe transition (HFAS), while ~35% are excited in the $2s \leftarrow 1s$ probe transition (H-REMPI). The excitation probability falls off rapidly with frequency detuning (FWHM ≈ 100 MHz).
[41] W. Demtröder, *Laser Spectroscopy: Volume 2: Experimental Techniques* (Springer-Verlag, Berlin, Heidelberg, 2008).
[42] J. K. Watson, J. Mol. Spectrosc. **207**, 276 (2001).
[43] G. B. Park, J. Chem. Phys. **141**, 134304 (2014).
[44] S.-K. Shih, S. D. Peyerimhoff, and R. J. Buenker, J. Mol. Spectrosc. **74**, 124 (1979).
[45] G. B. Ellison, private communication (2018).
[46] H. L. Berghout, F. F. Crim, M. Zyrianov, and H. Reisler, J. Chem. Phys. **112**, 6678 (2000).
[47] J.-C. Loison, S. H. Kable, P. L. Houston, and I. Burak, J. Chem. Phys. **94**, 1796 (1991).
[48] M. Tulej, G. Knopp, P. Beaud, T. Gerber, and P. Radi, J. Raman Spectrosc. **36**, 109 (2005).
[49] M. Zyrianov, T. Droz-Georget, and H. Reisler, J. Chem. Phys. **106**, 7454 (1997).
[50] E. A. Wannenmacher, H. Lin, and W. M. Jackson, J. Phys. Chem. **94**, 6608 (1990).
[51] M. Namai, T. Sasaki, H. Ishikawa, H. Morikuni, and N. Mikami, J. Phys. Chem. A **113**, 13081 (2009).
[52] Estimated lifetimes for the three HNCO $\tilde{A}$-state vibrational levels shown in Fig. 2 of Ref. 49.
[53] G. Herzberg, *Molecular Spectra and Molecular Structure. III. Electronic Spectra and Electronic Structure of Polyatomic Molecules* (D. Van Nostrand Company, 1966).